INTERNATIONAL JOURNAL OF CIRCUITS, SYSTEMS AND SIGNAL PROCESSING
DOI: 10.46300/9106.2021.15.162 Volume 15, 2021

Systematic structural and optical characterization of TiO_2 nanofibers synthesised by electrospinning

Oscar Secundino-Sánchez
UPIITA, Instituto Politécnico Nacional
Av. Instituto Politécnico Nacional 2580. La Laguna Ticomán, Ciudad de México. 07340.
México.

José F. Sánchez-Ramírez
Centro de Investigación en Biotecnología Aplicada, Instituto Politécnico Nacional.
Ex-Hacienda de San Juan Molino. Km 1.5 de la Carretera Estatal Santa Inés Tecuexcomac-Tepetitla. Tepetitla, Tlaxcala. 90700.
México.

Joel Diaz -Reyes
Centro de Investigación en Biotecnología Aplicada, Instituto Politécnico Nacional.
Ex-Hacienda de San Juan Molino. Km 1.5 de la Carretera Estatal Santa Inés Tecuexcomac-Tepetitla. Tepetitla, Tlaxcala. 90700.
México
Email: joel_diaz_reyes@hotmail.com

Received: March 20, 2021. Received: August 22, 2021. Accepted: September 17, 2021. Published: September 20, 2021.

Abstract—TiO_2 nanofibers were synthesised by means of the electrospinning technique, which were annealed at high temperatures to achieve the crystalline phase transformation. The chemical stoichiometry of electrospun TiO_2 nanofibers was estimated by EDS, finding that at low annealing temperatures excess of oxygen was detected and at high temperatures excess of titanium that originates oxygen vacancies. TEM images show clearly the formation of TiO_2 nanofibers (NF's) that exhibit a homogeneous and continuous aspect without the presence of crystalline defects, whose surface morphology depends strongly on the annealing temperature. The crystalline phase transformation was studied by Raman spectroscopy, which revealed that annealed TiO_2 NF's showed a crystalline phase transformation from pure anatase to, first a mix of anatase-rutile, then pure rutile as the annealing temperature increased, which was corroborated by X-ray diffraction and high-resolution TEM diffraction. The average grain size, inside the NF´s, increased with the crystalline phase transformation from 10 to 24 nm for anatase-TiO_2 and from 30 to 47 nm for rutile-TiO_2, estimated by using the Scherrer-Debye equation. The band gap energy (E_g), obtained from optical absorption spectra, decreases monotonically, where a local minimum is observed at 700 °C ranged in $3.75 \leq E_g \leq 2.42$ eV, caused by the anatase → rutile crystalline phase transformation. The photoluminescence shows that radiative bands show a gradual red-shift as the temperature increases due to the continuous change of E_g.

Keywords—Electrospinning technique, Semiconductor nanofibres, Titanium dioxide, Thermal treatment, crystalline phase transformation, optical properties

I. Introduction

THE synthesis of new semiconductor materials in nanometric size has received much attention in recent years because of the industrial demands increase [1], the number of reports on these nanoparticles such as nanofibers (NF's) has increased worldwide mainly on titanium dioxide [2]. Titanium dioxide (TiO_2) is a transition metal oxide that forms different polymorphs: rutile, anatase and brookite [3]. The most stable phases and, therefore, the most widely investigated are anatase and rutile, which are important for a wide variety of technological applications [4]. The low cost

and non-toxicity characteristics make TiO_2 ideal for use in photocatalysis [5]. Amorphous TiO_2 does not exhibit photocatalytic (PC) activity, thus, the crystallinity must be improved before PC applications [6]. Anatase is the most widely used phase in PC due to its high effectiveness in the degradation of organic pollutants [7,8]. The rutile phase of TiO_2 crystallizes in tetragonal structure whereas the anatase crystal phase in octahedral structure. The physicochemical properties of TiO_2 vary depending on the crystalline phases present in the material [9], and they also offer new properties when their dimensional scale is reduced to nanometric range [10]. The synthesis of one-dimensional nanostructures has been a subject of relevant importance in many areas of science, where new methods are sought every day for the manufacture or synthesis [11]. Unlike other nanostructures such as nanotubes, nanowires or nanorods, that are synthesized by chemical methods and generally require additional purifications that imply a higher cost, nanofibers (NF's) are manufactured using the electrospun technique, which turns out to be a highly efficient and low cost process [12]. The physical characteristics of electrospun-NF's, such as diameter and morphology, can be controlled depending on the final applications of the material. In recent years, the technique of electrostatic spinning or electrospinning has been worldwide actively investigated [13]. Electrospinning is a versatile technique that uses electrical forces to break the surface tension of the precursor solution and initiate the spinning process for the manufacture of fibers. This technique is capable of producing fibers with diameters in the nanometric range, reaching values below one nanometer [14]. Of the most outstanding properties of NF's is the high surface area. However, it is not the only one; a greater number of their physical properties can be exploited by carrying out a more detailed and systematic characterization of the morphological and structural properties. The diameter of electrospun TiO_2-NF's can be range controlled from one to hundreds of nanometers [15]. TiO_2-NF's produced by electrospinning have different properties as compared with other morphologies of the same material such as powders or films, furthermore, the NF's spacious morphology also provides great accessibility for liquid or gaseous reagents circulation [16,17].

In this research work, the controlled synthesis of electrospun TiO_2-NF's prepared with different crystalline structure and morphology are systematically analysed. The control of crystalline structures (anatase and rutile phases) and morphology properties were carried out through a heat treatment at high temperatures. The evaluation of the crystalline quality synthesis and structural/optical properties of the NF's were performed using the different characterization techniques such as X-ray Diffraction, Raman dispersion, TEM, HRTEM, UV-visible and photoluminescence at room temperature.

II. Experimental Details

To synthesize TiO_2-NF's the electrospinning technique was employed, following closely the method reported in ref. [18] but with some modifications in both the titanium molecular precursor and in amount of PVP used. By thermal treatment (TT) of each TiO_2-NF sample in the temperature range of 100-1000 °C (with a precision ±2 °C) for 2 h in an oven (trademark Barnstead Thermolyne 1300 Furnace), in an air atmosphere, the crystal phase transformation from pure anatase to anatase-rutile mixed and, finally, to pure rutile was achieved. For TT of electrospinning TiO_2-NF's a special gas mixture as oxidation atmosphere was not used, but it was performed in the laboratory air atmosphere. The oxidation temperature used increase was 4 °C/min, and after annealing, they were allowed to cool to room temperature (RT) for later characterization. The precursors utilized to synthesise the TiO_2-NF's were titanium (IV) n-butoxide (TBT, $(Ti(OBu)_4$, (Mw= 340.32 g/mol with 97 % purity) and polyvinylpyrrolidone (PVP, M_W = 1300000 g/mol with 99.9 % purity) purchased from Sigma-Aldrich company, glacial acetic acid and ethanol from Baker supplier. All chemicals precursors were used as they were provided without subsequent purification. Distilled and deionized water (>18 MΩ cm^{-1}) was used all the time to wash the laboratory equipment employed during the NF´s preparation. After annealing a set of eleven samples were obtained, tagged from M0 to M10 as TT changed from 0 to 1000 °C in steps of 100 °C. The stoichiometry of titanium dioxide nanofibers were measured electron dispersive spectroscopy (EDS) in a LEO 438VP with WD system of 26 mm using a pressure of 20 Pa. Raman scattering experiments were performed at RT using a Raman Thermo Scientific brand DXR smart spectrometer with an operating range of 50-3350 cm^{-1} and a 780 nm laser excitation source with 12 mW output power and a thermoelectrically cooled CCD detector. Typical spectrum acquisition time was limited to 60 s to minimize the sample heating effects. The Raman shift and the full width at half-maximum (FWHM) of each peak have been determined by a quantitative fit to the experimental Raman spectra using a sum of Lorentzian line distributions. First dominant peaks were fit, and the additional peaks were added as necessary. The TiO_2-NF's crystalline phase and structural quality were determined measuring X ray diffraction (XRD) patterns with a Bruker D8 Discover diffractometer using the copper Kα radiation (λ=0.15406 nm) at 40 kV and 40 mA with parallel beam geometry in steps of 0.02°. The morphology, selected area electron diffraction (SAED) and high-resolution transmission electron microscopy (HRTEM) studies were carried out in a JEOL JEM200 of 80-200 kV, the obtained images are recorded with a CCD camera in real time. The Gatan Digital Micrograph software was used for the analysis of HRTEM images. High-resolution electron microscope (HRTEM) images were digitally processed by using filters in the Fourier space. For electron microscopy analysis, two microscopes, a Jeol JEM200 and a Tecnai 200 TEM were employed for the observations of the samples with low-magnification and high-resolution, respectively. RT optical absorption spectra of the colloidal samples were recorded using a 10 mm path length quartz cuvette in a UV-Vis-NIR scanning spectrophotometer (Shimadzu UV 3101PC double beam). The RT photoluminescence was measured using a He-Cd (Omnichrome–Series 56) laser emitting at 325 nm with an optical excitation power of ~15 mW. The radiative emission from the sample was focalized to the entrance slit of a HRD-100 Jobin-Yvon double monochromator, with a resolution better than 0.05 nm, and detected with an Ag-Cs-O

Hamamatsu photomultiplier with a spectral response in the 350-1000 nm range.

III. Experimental Results and Discussion

TEM images of three typical annealed TiO_2-NF's are shown in Fig. 1: M1, M5 and M10 samples, which show clearly the presence of solid nanofibres with a well-defined shape and without the presence of interconnections and defects as beads, ribbon-like and pores along the longitudinal direction. In the TEM images, the TT effect on the nanofibers surface morphology and diameter is clearly observed. They present a smooth surface and are thick at low annealing temperatures (AT's), as the temperature augments they become rough and segmented and the diameter decreases. Fig. 1 shows TEM images of a TiO_2-NF sample where nanometric diameters are evident. Based on the diameters measurements, taken from the TEM images, histograms of diameter distribution were obtained that allowed to estimate the mean diameter of each sample, the results are presented in Table 1 and in the inset of Fig. 1, which clearly show two behaviors for the TiO_2 NFs diameter: 1) for the AT ≤ 500 °C, the decrease is exponential with an activation energy of 38.93 meV that can associate with the oxygen desorption energy. 2) For AT > 500 °C the diameter remains almost constant. From these results it is observed that the average diameter depends strongly on AT.

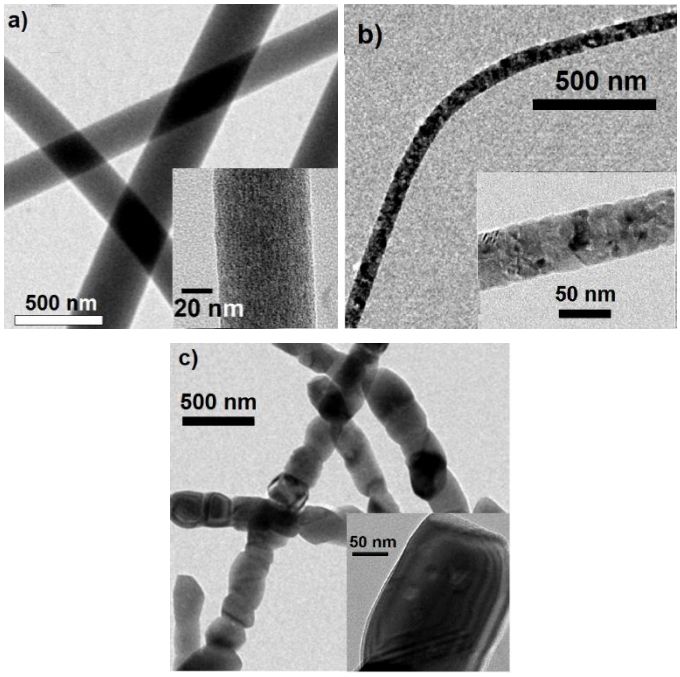

Fig.1. TEM images of three typical electrospun TiO_2-NF's annealed at a) 0, b) 500 and c) 1000 °C, respectively. The insets show high magnification image taken from the surface morphology.

Table 1. Annealing temperature of electrospun TiO_2-NF's samples. Diameters are also included.

Sample	Annealing temperature (°C)	Nanofiber diameter (nm)
M0	0	137.00 ± 0.42
M1	100	128.00 ± 0.39
M2	200	120.05 ± 0.37
M3	300	117.50 ± 0.36
M4	400	116.00 ± 0.35
M5	500	114.62 ± 0.35
M6	600	115.00 ± 0.35
M7	700	115.40 ± 0.35
M8	800	115.00 ± 0.35
M9	900	115.00 ± 0.35
M10	1000	115.30 ± 0.35

The systematic study of the chemical composition of annealed TiO_2-NF's was carried out by EDS. The results obtained for titanium and oxygen of all the studied samples are illustrated in Fig. 2. From figure a monotonic decrease/increase of the oxygen/titanium molar fraction is observed, until reaching the ideal stoichiometric composition around AT = 500 °C, for higher temperatures the data stay practically constant. The decrease in the molar fraction of oxygen with the increase of AT indicates the generation of oxygen vacancies (V_{Ox}'s). In addition, at low temperatures a strong dependence of the oxygen and titanium molar concentrations on AT is observed in Fig. 2. These experimental results can be explained as follows: the as-synthesized TiO_2-NF's are amorphous, which contain a large amount of residual impurities that come from the employed precursors and from the PVP carrier. When TiO_2-NF's are heated at high temperatures, the PVP and most residual impurities are desorbed. Furthermore, V_{Ox}'s are generated and the atoms in the crystal lattice rearrange to form the crystalline phases (CP's) of TiO_2, causing a decrease in the diameter of TiO_2-NF's. The TiO_2 crystalline structure is tetragonal for both crystalline phases, anatase and rutile, thus, the atomic weight of the ideal TiO_2 unit cell is ~ 159.796 u, from which 40.049% corresponds to oxygen atoms and 59.951% to titanium atoms. It is observed from Fig. 2 that the sample annealed at 500 °C is the one with the best chemical stoichiometry as compared to the ideal molar concentrations. From this, one observes that TiO_2-NF's annealed at temperatures below 500 °C contain a higher concentration of oxygen atoms, indicating that these ones can be found in interstices and antisites in the TiO_2 unit cell, which cause a high concentration of structural defects. As the temperature increases, oxygen atoms are desorbed creating V_{Ox}'s, which in turn cause the crystalline phase transformation, as will be discussed later. Consequently, remains a lower molar fraction of oxygen atoms in this temperature range, indicating thus a high concentration of V_{Ti}'s. At AT's > 500 °C great variation in the incorporation of titanium atoms in the lattice or the desorption of oxygen atoms is no longer produced, which also indicates that, in this range of temperatures, large production of V_{Ox}'s is no longer generated. As seen in Fig. 2, for AT´s > 500 °C the mole fractions vary slightly and remain close to the stoichiometric molar fractions. Therefore, low-temperature annealing of TiO_2-NF's originate high oxygen desorption, so originating V_{Ox}'s. Furthermore, it causes the reduction of the

nanofiber diameter and, most important, the CP transformation.

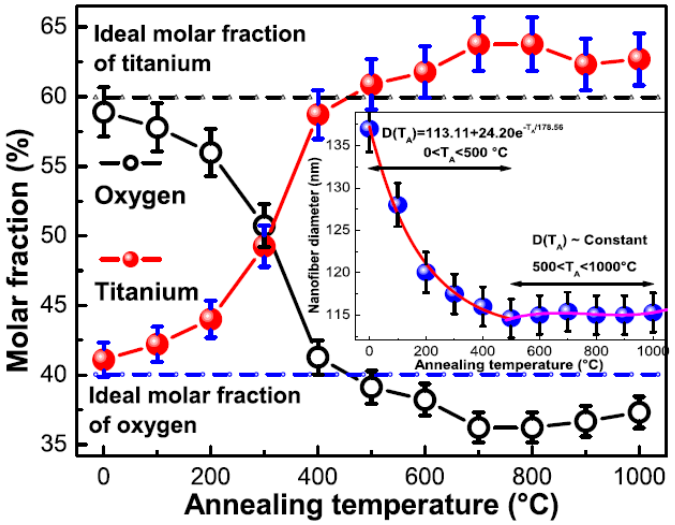

Fig. 2. Chemical stoichiometry of the electrospun TiO_2 as function of the AT. The inset depicts NF's diameter versus AT's.

In order to determine the crystalline phase and structural quality of TiO_2, Raman scattering and X-ray diffraction (XRD) analysis of the samples were performed. As is showed by Raman spectroscopy in the 80-800 cm^{-1} interval, the as-synthesised TiO_2-NF's are amorphous and become crystalline after annealing at determined high temperature in an air atmosphere, which causes the annealed NF's to transform the crystalline structure from amorphous → anatase → anatase-rutile mixed → rutile [19] (see Fig. 3A)). Fig. 3B illustrates four typical Raman spectra (M5, M6, M8 and M9) that allow to clearly observe the vibrational bands associated to the different CP's, also the structural quality of the annealed samples. Additionally, it can be observed that there is a critical temperature at which the transformation to CP occurs, normally ~560 °C [19]. The M5 sample (AT = 500 °C) Raman spectrum (a) in Fig. 3B, shows four vibrational bands at 142, 397, 518 and 634 cm^{-1}, corresponding to the Raman modes $E_g(\nu_1)$, $B_{1g}(\nu_3)$, $A_{1g}(\nu_4)$ and $E_g(\nu_6)$; associated to the anatase CP [20]. Fig. 3B shows the (d) Raman spectrum of the M9 sample (AT = 900 °C) that presents vibrational modes at 142, 232, 445 and 610 cm^{-1} that are assigned to A_{1g}, E_g, multi-phonon process and B_{1g}, respectively, associated to the Raman active modes (RAM's) of rutile CP. In this figure, the (b) and (c) Raman spectra (AT = 600, 800 °C) present a mixture of RAM's associated with both CP's, in the first spectrum anatase dominates and in the second one rutile. Based on these results, the CP transformation of the TiO_2-NF´s annealed at different temperatures can be systematically followed and clearly discussed. Furthermore, the Raman spectrum of M2 sample (AT = 200 °C), despite the fact that most TiO_2 is amorphous, shows a slight crystallinity, since the RAM $E_g(\nu_1)$ associated

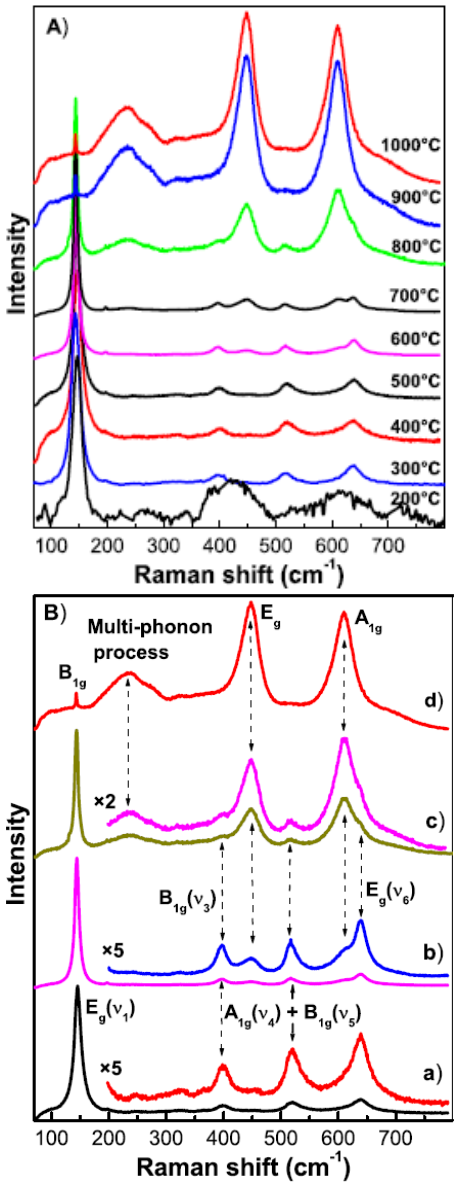

Fig. 3. A) Raman spectra of the TiO_2-NF's annealed at different temperatures. B) Raman spectra of samples annealed at a) 500, b) 600, c) 800 and d) 900 °C. Weak vibrational bands are magnified (and superimposed) for a better comparison.

with the anatase phase is present with FWHM = 19.7 cm^{-1}. At AT's > 200 °C the phase crystalline quality (CQ) of samples improves appreciably, and the other RAM's characteristic of the crystalline anatase begin to appear. At AT = 500 °C, RAM's associated with the anatase phase are well-resolved and the FWHM of the dominant active mode $E_g(\nu_1)$ is ~ 15.6 cm^{-1}, which indicates a better CQ. At AT = 600 °C, the rutile phase begins to emerge coexisting with the anatase phase (see Fig. 3), until the rutile CP becomes dominant as observed in the spectrum of the M8 sample (AT = 800 °C). This fact indicates that in the range from 500 to 600 °C there is a critical temperature, at around 560 °C [19], where the anatase → rutile CP transformation starts, caused by the generation of V_{Ox}'s. For AT's > 800 °C, the rutile is the only CP present as Raman spectra reveal, since only RAM's of this CP are

present (see Fig. 3). This CP behaviour is explained based on the EDS results of Fig. 2. As observed when AT = 700 °C, the oxygen molar fraction no longer varies appreciably, indicating that there is no more Vo_x's large generation and therefore there is no CP transformation anymore, only rutile remains. Additionally, CQ of rutile can be evaluated as a function of AT by estimating the FWHM of the dominant A_{1g} (608.3 cm^{-1}) and E_g (444.15 cm^{-1}) RAM's. For AT = 600 °C the FHWM of A_{1g} mode equals 56.93 cm^{-1} and FHWM of E_g one = 33.14 cm^{-1}. As AT increases the FWHM gradually decreases to 35.56 cm^{-1} for A_{1g} and to 32.20 cm^{-1} for E_g, both when AT = 800 °C. These values indicate that the M8 sample has a better CQ than the rutile fraction contained in the M6. For higher AT's the average widths do not vary appreciably, which means that the CQ is maintained at least up to 1000 °C annealing. With these discussed results can say the synthesised material at 500 and 800 °C have a good CQ for anatase and rutile, respectively. These results were corroborated by XRD and HRTEM, which are then discussed.

The multi-peaks diffractions observed in the XRD patterns of Fig. 4 indicate that the TiO_2-NF's are of polycrystalline nature. In figure, the XRD patterns of four typical TiO_2-NF's obtained at different AT's are presented. In Fig. 4a diffractogram of the M5 sample shows diffraction peaks at 2θ = 25.24, 37.69, 48.02, 53.84, 54.23 and 62.70°, which correspond to the crystalline planes (101), (004), (200), (105), (211) and (204), respectively, of anatase CP (JCPDS cards # 00-021-1272). In addition, other weak peaks were also identified on patterns. The diffractogram of the M10 sample (Fig. 4d) exhibits main diffraction peaks at 2θ = 27.37, 36.00, 54.40 and 56.55° that are associated to the crystalline planes (110), (101), (211) and (220) of rutile CP (JCPDS cards # 00-021-1276). Additionally, in XRD patterns of the M10 sample weak diffraction peaks are present, which were also identified and labelled. Fig. 4b shows the XRD pattern of M7 sample, which clearly exhibits peaks of both CP´s, that is, anatase-rutile mixed. Finally, Fig. 4c shows M8 diffractogram, which shows the main diffraction peaks of rutile and weak peaks associated to anatase, as was also seen by Raman scattering. In addition, the weak peaks of both diffractograms were multiplied by a numerical factor for magnification, which were deconvoluted and assigned to each CP by means the databases above mentioned (see insets in Fig. 4). This indicates that there are no longer CP transformations despite AT increases. Diffractograms show that at low AT values the formation of the anatase (A) is promoted while at the other extreme the rutile (R) crystalline structure dominates. It is observed that in the 500-600 °C range the A→R transition occurs, where the exact critical temperature T_{Ac}, as has been previously reported, is about 560 °C [19]. Notice that the preferential growth direction is (101) for anatase and (110) for rutile. It is observed that the FWHM of the main peak in the XRD patterns decreases as AT increases, indicating that the average diameter of the nanocrystals that make up the TiO_2-NF's increases when AT increases. The average crystallite size of the nanoparticles of the annealed TiO_2-NF's was estimated by applying the Scherrer-Debye equation to the dominant peak of the diffraction data and taking the average value [21,22]. The results are illustrated in Fig. 5, for the two CP´s and for anatase-rutile mixed. It was found that anatase structure transformed to the rutile phase after reaching certain nanoparticle size, with the rutile phase turning more stable than anatase for particle sizes greater than 14 nm [23]. For AT = 500 °C a grain size of 13.65 nm is obtained, for a higher temperature the grain size exceeds 14 nm; therefore, the CP transformation occurs (see Fig. 5). Once the rutile phase was formed, its nanocrystals grew faster than anatase phase. By refining experimental XRD data the parameters of anatase and rutile unit cells can be calculated taking into account that both crystalline structures are tetragonal. The results are shown in the inset of Fig. 5, which are closely similar to those of bulk TiO_2 (for anatase a_{bulk} = 3.7845, c_{bulk} = 9.5143 Å and for rutile a_{bulk} = 4.5937 Å, c_{bulk} = 2.9587 Å), as can be seen in figure only the anatase phase is slightly stressed.

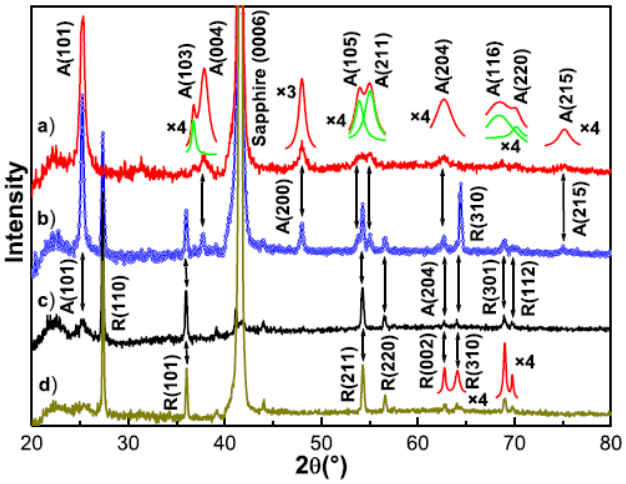

Fig. 4. X-ray diffractograms of the annealed samples: a) M5, b) M7, c) M8 and d) M10. The peaks are labelled using standard crystallographic cards (JCPDS cards # 00-021-1272) for anatase, and (JCPDS cards # 00-021-1276) for rutile.

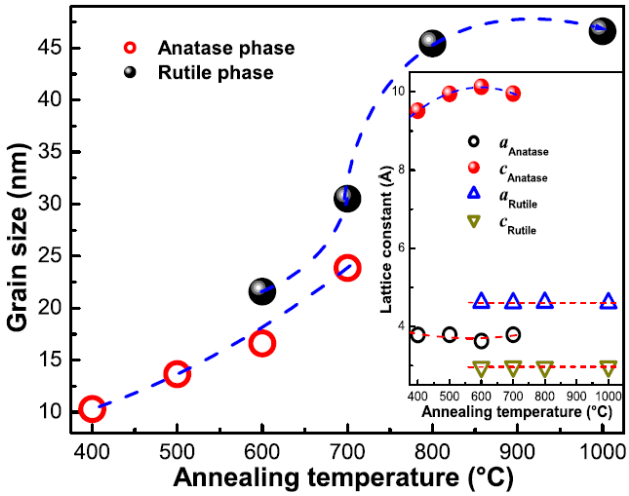

Fig. 5. The TiO_2-NF's grain size as function of the annealing temperature. The inset presents the lattice constants as function of the annealing temperature for both crystalline phases.

With the aim to verify the structure´s quality and CP of the prepared electrospun TiO_2-NF's, HRTEM images were taken and the results are included in Fig. 6, that shows high-resolution TEM images taken from different parts of four typical annealed TiO_2-NF's, which shown the presence of anatase and rutile titania. Fig. 6a displays a high-resolution TEM image showing the anatase grains in the M5-NF (AT = 500 °C). Amplifying and analysing the selected area of the micrograph (shown as inset in Fig. 6a) suggests that the 0.359 nm *d*-spacing corresponds to the (101) anatase crystal planes. The corresponding SAED pattern (inset image in Fig. 6a) indicates that the nanoparticles are polycrystalline anatase, in good agreement with the XRD results. Similarly, Fig. 6d shows evidence of (110) rutile planes. Figs. 6b-c present evidences of both CP's, these results support the previous analysis that the produced TiO_2-NF's have a polycrystalline anatase-rutile mixed phase structure, caused by thermal heating in the AT 600-800 °C range as observed by Raman scattering and XRD.

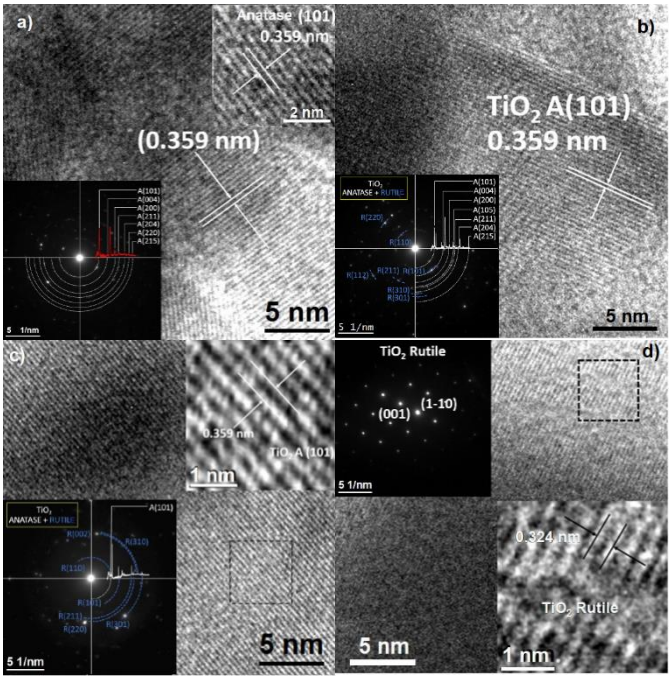

Fig. 6. TEM images and corresponding SAED patterns (inset) of TiO_2-NF's synthesized by electrospinning technique annealed at different temperatures: a) 500, b) 700, c) 800 and d) 1000 °C, respectively.

The effect of TT´s on the band gap energy (E_g) of electrospinning TiO_2-NF's was investigated by RT absorbance (optical density: OD). E_g variation as function of the AT's was calculated from optical absorption data. Fig. 7 depicts, for three typical samples (M5, M6 and M9), the first derivative of the optical density [$d(OD)/d(h\nu)$] as a function of the incident photon energy ($h\nu$, Plank constant times frequency). The relative minima in the *d(OD)/d(Energy)* spectra versus $h\nu$ graph defines with excellent approximation the various critical points of the band structure. Fig. 7 evidences, for the three representative samples, the E_g position-change in the energy axis [24]. The separation among E_g for M5, M6 and M9 (AT = 500, 600 and 900 °C, respectively) observed in Fig. 7, for the

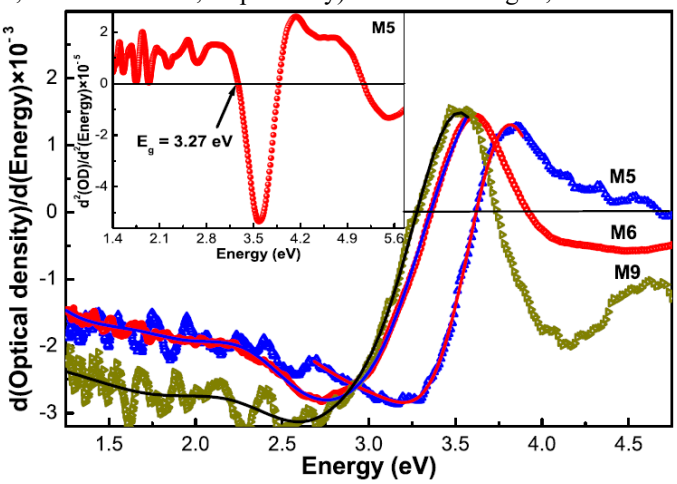

Fig. 7. First derivative of the optical absorption (*OD*) as a function of the photon energy ($h\nu$) for three different ATs. The inset displays the second derivative of *OD* versus $h\nu$, which allows to calculate E_g for M5. The arrow indicates the position of E_g.

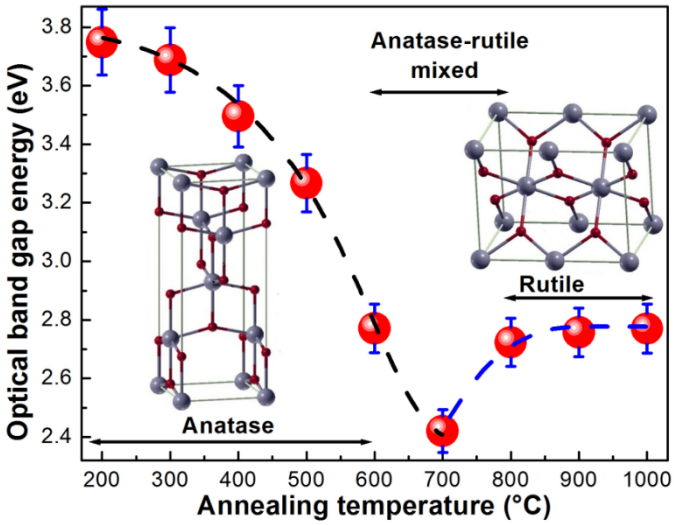

Fig. 8. Band gap energy of the TiO_2-NF´s as a function of annealing temperature. Besides, anatase and rutile lattices are included as insets.

three typical samples, denotes a good indication of the size change in the lattice parameter of the structure associated to the CP transformation [25]. The inset in Fig. 7 shows the second derivative of *OD* plotted against Energy. A more exact position of the critical point E_g in the Energy-axis is defined by the crossing of the second derivative curve with the Energy-axis, or rather the zero-position, which is pointed out by the upward arrow. The band gap energy obtained for the AT = 500 °C was 3.27 ± 0.08 eV. Similar analyses were performed for the rest of the annealed nanofibers and the obtained results are presented in Fig. 8. The band gap energy, obtained from optical absorption spectra, decreases monotonically but a local minimum is observed at T_A = 700 °C, and then goes back up slightly keeping almost a constant value, which corresponds to the rutile CP (see Fig. 8). To explain this band-gap energy behaviour, the aforementioned

results will be used. In the 200-600 °C AT-range a high density of V_{Ox}'s coming from the anatase phase is generated, and a decrease of E_g occurs, in addition, the crystalline domain increases. In the 600-800 °C AT-range, where anatase and rutile coexist, E_g vs AT exhibits a local minimum. This minimum can be due to the disorder in the anatase-rutile crystalline system, which reduces the band gap in a similar way as reported by other materials [25]. Finally, in the 800-1000 °C AT-range only rutile phase exists, where no more V_{Ox}'s are generated and no CP transformation happens, E_g remains almost constant, (see Fig. 8). TiO_2-NF's annealed up to 300 °C possess optical E_g's greater than 3.69 eV; these values may be unreliable because of a relatively high proportion of the limit volume of amorphous grains [26,27], unless a small fraction of the crystalline domain is responsible, as was seen in the M3 sample by Raman scattering. For samples annealed at 400 °C E_g ~3.50 eV and at 500 °C ~3.27 eV [28,29]; these E_g values are relatively representative for well-crystallised anatase phase. At AT's > 500 °C, E_g decreases until reaching ~2.42 eV at 700 °C as local minimum; which still represents another value reported for anatase-rutile mixed of unknown relative proportions, which is associated to V_{Ox}'s generated by TT, and probably with some carbon contamination from PVP origin [30,31]. For AT > 800 °C, the NF's-E_g remains almost constant in the 2.72-2.77 eV interval, this result is probably a relatively representative value for well-crystallised rutile. It is important to consider that the range of values for E_g's of the crystalline anatase and rutile generally reported in the literature is larger than the ones measured in this work. However, values reported here are valid since for anatase values in the range $3.20 \leq E_g \leq 3.56$ eV have been reported by other authors [32-34]. For rutile, $3.00 \leq E_g \leq 3.34$ eV is a typical range [32,35,36]. For an anatase and rutile mixed few reports were found about E_g, where the 3.11-3.17 eV interval contains the most values [27,32,33]. For this system E_g = 3.75 eV was measured for AT = 200 ºC, which may be due to the small fraction of anatase-TiO_2 nanocrystals synthesised at that temperature [37]. This value is higher than the more common E_g = 3.2 eV. E_g = 3.27 eV is approximately that of bulk TiO_2 obtained when AT ~ 500 ºC.

Figure 9 shows the RT photoluminescence (PL) spectra for NF's with AT in the 200-1000 °C range, in which is clearly observed the PL emission of electrospinning TiO_2-NF's achieved by structural phase transformation. In this work, the titanium precursor employed is TBT, which is a precursor product of highly reactive metallic alkoxide due to the highly reactive alkoxide (OR) groups presence. The TiO_2 synthesis procedures lead to the formation of alkoxy (Ti-OR) groups [38-40] on the TiO_2 nanoparticles surface, in which seem that Ti-OR groups passivate surface traps, thus promoting the radiative recombinations [41]. Fig. 9 illustrates that nanofibres with AT < 400 °C present two radiative transitions, although with very wide FWHM, which is indicative of a poor crystalline quality of the TiO_2 nanofibres as previously was discussed by Raman scattering. These weak radiative transitions are due to anatase-TiO_2 nanocrystals formed in those nanofibers, which may be caused by deep impurities and structural defects. Similarly, the M5 sample shows a dominant radiative band at 1.98 eV, and other weak broad band at 1.40 eV, obtained by deconvolution, associated to surface traps levels induced by oxygen excess [41,42] and/or carbon complexes as the alkoxides [41], where the redshift is due to the E_g decrease. For 600 ≤ AT ≤ 800 °C, the mix anatase-rutile synthesises, whose PL spectra depend strongly on the dominant CP. The only PL spectrum where both CP's are manifested is that of M6 sample, which presents three PL bands at 2.56, 2.04 and 1.44 eV. The first two are associated to anatase and the last one to rutile. Furthermore, for AT > 700 °C, only the rutile phase PL spectrum prevails, which has four luminescent bands (see Fig. 9). Unlike the PL spectra of anatase, the PL spectra of rutile do not change appreciably, as is shown in Fig. 9, despite AT increased from 700 to 1000 °C, corroborating that V_{Ox}'s are no longer generated, as was observed by EDS, which promote the CP transformation. The redshift of anatase and rutile NF's luminescent emissions, is caused by the E_g reduction as result of CP transformation, since the energy-levels of the shallow traps due to V_{Ox}'s are the same in both crystalline structures. The RT PL spectra of the anatase-TiO_2-NF's show two radiative bands, which could correspond to free electron-to-acceptor or donor-to-acceptor recombination and are associated with alkoxide and deep defects associated to V_{Ox}'s [41]. Finally, the PL spectra of the rutile-TiO_2-NF's exhibit four PL bands at 1.35, 1.37, 146 and 1.51 eV, which could be caused by the alkoxides and deep defects associated to V_{Ox}'s as has been already reported [41].

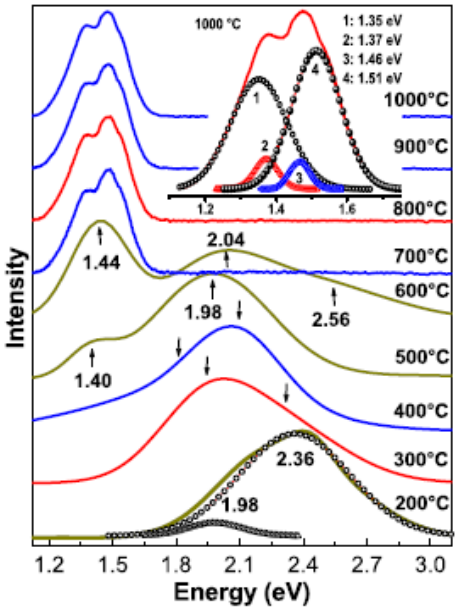

Fig. 9. Photoluminescence spectra of the samples annealed at the temperature range 200-1000°C.

IV. Conclusions

In this work a systematic study of preparation and characterization of electrospun TiO_2 nanofibers (NF's) is reported. From as-prepared amorphous TiO_2 the crystallization and changes of phases along the thermal treatments in the 100

– 1000 °C interval in air, the morphological, structural and optical properties are studied. As confirmed by XRD and Raman scattering measurements, amorphous-crystalline TiO_2 constitutes the NF's, in the annealing temperature (AT) 200 - 500 °C interval anatase is the predominant phase, a mix of anatase and rutile coexists in the $500 \leq E_g \leq 800$ °C, and the rutile phase is predominant for AT > 800 °C. TEM images show the TiO_2-NF's free of crystalline defects. Energy band gap (E_g) decreases gradually from 3.75 eV (AT = 0) up to 2.4 eV (AT = 700 °C), from where increases until ~3.8 eV for AT = 1000 °C. Photoluminescence spectra show how the crystalline quality (CQ) gradually improves from AT = 0 to 1000 °C, where TiO_2 is completely crystallized, in practice, for rutile. From PL spectra is observed that anatase (with some small contribution of rutile) exhibits the best crystalline quality when AT = 600 °C. In summary, this study shows how the electrospun TiO_2 NF's gradually change of phases when are annealed in air in the 0 – 1000 °C range, and the gradual variation of the physical properties. Furthermore, it is shown that the TiO_2 NF´s prepared by electrospun are ideal for application photocatalyst using visible radiation because a best CQ and an appropiate E_g value for AT = 600 °C.

A. References

[1] S. Riaz, S. Naseem. Controlled nanostructuring of TiO_2 nanoparticles: a sol–gel approach. *J. Sol-Gel Sci. Technol*. 74(2015) 299–309.

[2] Kenry, C. T. Lim. Nanofiber technology: current status and emerging developments. *Prog. Polym. Sci.* 70 (2017) 1–17.

[3] R. Hada, A. Amritphale, S. S. Amritphale, S. Dixit. A Novel Mixed Reverse Microemulsion Route for the Synthesis of Nanosized Titania Particles. *The Open Mineral Processing Journal* 3 (2010) 68-72.

[4] D. A. H. Hanaor, C. C. Sorrell. Review of the anatase to rutile phase transformation. *J. Mater. Sci*. 46 (2011) 855–874.

[5] I. K. Konstantinou, T. A. Albanis. TiO_2-assisted photocatalytic degradation of azo dyes in aqueous solution: kinetic and mechanistic investigations: A review. *Appl. Catal. B* 49 (2004) 1−14.

[6] S. H. Othman,S. A. Rashid,T. I. M. Ghazi, N. Abdullah. Fe-Doped TiO_2 Nanoparticles Produced via MOCVD: Synthesis, Characterization, and Photocatalytic Activity. *J. Nanomater*. 2011 (2011) 8 pages.

[7] J. M. Herrmann, Ch. Guillard, J. Disdier, C. Lehaut, S. Malato, J. Blanco. New industrial titania photocatalysts for the solar detoxification of water containing various pollutants. *Appl. Catal. B* 35 (2002) 281–294

[8] R. F. Howe. Recent Developments in Photocatalysis. *Asia-Pac. J. Chem. Eng.* 6 (1998) 55-84.

[9] R. Chandrasekar, L. Zhang, J. Y. Howe, N. E. Hedin, Y. Zhang, H. Fong. Fabrication and characterization of electrospun titania nanofibers. *J. Mater. Sci*. 44 (2009) 1198–1205.

[10] A. P. Alivisatos. Perspectives on the Physical Chemistry of Semiconductor Nanocrystals. *J. Phys. Chem.* 100 (1996) 13226–13239.

[11] J. Jeevanandam, A. Barhoum, Y. S. Chan, A. Dufresne, M. K. Danquah. Review on nanoparticles and nanostructured materials: history, sources, toxicity and regulations. *Beilstein J. Nanotechnol*. 9 (2018) 1050–1074.

[12] A. Kumar, R. Jose, K. Fujihara, J. Wang, S. Ramakrishna. Structural and Optical Properties of Electrospun TiO_2 Nanofibers. *Chem. Mater.* 19 (2007) 6536–6542.

[13] Z. Huang, Y. Z. Zhang, M. Kotaki, S. Ramakrishna. A review on polymer nanofibers by electro-spinning applications in nanocomposites. *Compos. Sci. Technol*. 63 (2003) 2223-2253.

[14] S. Jian, J, Zhu, S. Jiang, S. Chen, H. Fang, Y. Song, G. Duan, Y. Zhang, H. Hou. Nanofibers with diameter below one nanometer from electrospinning. *RSC Adv*. 8 (2018) 4794–4802

[15] D. H. Reneker, I. Chun. Nanometre diameter fibres of polymer, produced by electrospinning. *Nanotechnology* 7 (1996) 216-223

[16] A. Frenot, I. S.Chronakis. Polymer nanofibers assembled by electrospinning. *Curr. Opin. Colloid interface Sci.* 8 (2003) 64-75.

[17] V. Thavasi, G. Singh, S. Ramakrishna. Electrospun nanofibers in energy and environmental applications. *Energy Environ. Sci.* 1 (2008) 205–221.

[18] D. Li, Y. Xia. Fabrication of Titania Nanofibers by Electrospinning. *Nano Lett*. 3 (2003) 555-560.

[19] O. Secundino-Sánchez, J. Díaz-Reyes, J. Águila-López, J. F. Sánchez-Ramírez. Crystalline phase transformation of electrospinning TiO2 nanofibres carried out by high temperature annealing. *J. Mol. Struct*. 1194 (2019) 163-170

[20] H. L. Ma, J. Y. Yang, Y.Dai, Y. B. Zhang, B. Lu, G. H. Ma. Raman study of phase transformation of TiO_2 rutile single crystal irradiated by infrared femtosecond laser. *Appl. Surf. Sci*. 253 (2007) 7497-7500.

[21] M. K. Singh, A. Agarwal, R. Gopal, R. K. Swarnkar, R. K. Kotnala. Dumbbell shaped nickel nanocrystals synthesized by a laser induced fragmentation method. *J. Mater. Chem.* 21 (2011) 11074-11079.

[22] J. Díaz-Reyes, J. I. Contreras-Rascón, J. S. Arias-Cerón, J. F. Sánchez-Ramírez, M. Galván-Arellano, J. Martínez-Juárez, J. A. Balderas-López. Structural and optical characterisation of $CdSe_{1-y}S_y$. *Mater. Sci. Semicond. Process*. 37 (2015) 199-206.

[23] Q. Zhang, L. Gao, J. Guo. Effects of calcination on the photocatalytic properties of nanosized TiO_2 powders prepared by $TiCl_4$ hydrolysis. *Appl. Catal. B* 26 (2000) 207-215.

[24] M. E. Linares-Avilés, J. I. Contreras-Rascón, J. Díaz-Reyes, J. Martínez-Juárez, R. S. Castillo-Ojeda, M. Galván-Arellano, J. A. Balderas-López, M. Álvarez-Ramos. Characterization of CBD-CdS Doped with Some Rare Earths III (Eu^{3+},Ce^{3+}) as Function of Synthesis Time. *Mater. Res.* 21 (2018) e20170626.

[25] A. Rivera-Márquez, M. Rubín-Falfán, R. Lozada-Morales, O. Portillo-Moreno, O. Zelaya-Angel, J. Luyo-Alvarado, M. Meléndez-Lira, L. Baños. Quantum Confinement and Crystalline Structure of CdSe Nanocrystalline Films. *Phys. Stat. Sol. (a)* 188 (2001) 1059–1064.

[26] Z. Wang, U. Helmersson, P.O. Käll. Optical properties of anatase TiO_2 thin films prepared by aqueous sol–gel process at low temperature. *Thin Solid Films* 405 (2002) 50–54.

[27] A. Nakaruk, D. Ragazzon, C.C. Sorrell, Anatase–rutile transformation through hightemperature annealing of titania films produced by ultrasonic spray pyrolysis. *Thin Solid Films* 518 (2010) 3735–3742.

[28] C. Kuchi, G. S. Harish, P. S. Reddy. Effect of polymer concentration, needle diameter and annealing temperature on TiO_2-PVP composite nanofibers synthesized by electrospinning technique. *Ceram. Int*. 44 (2018) 5266–5272.

[29] O. Frank, M. Zukalova, B. Laskova, J. Kürti, J. Koltai, L. Kavan. Raman spectra of titanium dioxide (anatase, rutile) with identified oxygen isotopes (16,17,18). *Phys. Chem. Chem. Phys.* 14 (2012) 14567–14572.

[30] L. Jing, B. Xin, F. Yuan, L. Xue, B. Wang, H. Fu. Effects of surface oxygen vacancies on photophysical and photochemical processes of Zn-doped TiO_2 nanoparticles and their relationships. *J. Phys. Chem. B* 110 (2006) 17860–17865.

[31] M. A. Hamid, I. A. Rahman. Preparation of titanium dioxide (TiO_2) thin films by sol gel dip coating method. *Malay. J. Chem*. 5 (2003) 086–091.

[32] D. Mardare, M. Tasca, M. Delibas, G. I. Rusu. On the structural properties and optical transmittance of TiO_2 r.f. sputtered thin films. *Appl. Surf. Sci*. 156 (2000) 200–206.

[33] H. H. Huang, C. C. Huang, P. C. Huang, C. F. Yang, C. Y. Hsu. Preparation of rutile and anatase phases titanium oxide film by RF sputtering. *J. Nanosci. Nanotechnol*. 8 (2008) 2659–2664.

[34] L. Miao, P. Jin, K. Kaneko, A. Terai, N. Nabatova-Gabain, S. Tanemura. Preparation and characterization of polycrystalline anatase and rutile TiO_2 thin films by rf magnetron sputtering. *Appl. Surf. Sci*. 212–213 (2003) 255–263.

[35] C. C. Ting, S. Y. Chen, D. M. Liu. Structural evolution and optical properties of TiO_2 thin films prepared by thermal oxidation of sputtered Ti films. *J. Appl. Phys.* 88 (2000) 4628–4633.

[36] H. Tang, K. Prasad, R. Sanjinès, P.E. Schmid, F. Lévy. Electrical and optical properties of TiO_2 anatase thin films. *J. Appl. Phys*. 75 (1994) 2042–2047.

[37] S. Valencia, J. M. Marín, G. Restrepo. Study of the bandgap of synthesized titanium dioxide nanoparticles using the sol-gel method and a hydrothermal treatment. *Open Mater. Sci. J*. 4 (2010) 9–14.

[38] M. Niederberger, M. H. Bartl, G. D. Stucky. Benzyl alcohol and titanium tetrachloride–A versatile reaction system for the nonaqueous and low-temperature preparation of crystalline and luminescent titania nanoparticles. *Chem. Mater*. 14 (2002) 4364–4370.

[39] Y. Zhu, C. Ding, G. Ma, Z. Du. Electronic state characterization of TiO_2 ultrafine particles by luminescence spectroscopy. *J. Solid State Chem*. 139 (1998) 124–127.

[40] W. F. Zhang, M. S. Zhang, Z. Yin, Q. Chen. Photoluminescence in anatase titanium dioxide nanocrystals. *Appl. Phys. B* 70 (2000) 261–265.

[41] N. D. Abazović, M. I. Čomor, M. D. Dramićanin, D. J. Jovanovicć, S. P. Ahrenkiel, J. M. Nedeljković. Photoluminescence of anatase and rutile TiO_2 particles. *J. Phys. Chem. B* 110 (2006) 25366–25370.

[42] N. Daude, C. Gout, C. Jouanin. Electronic band structure of titanium dioxide. *Phys. Rev. B* 15 (1977) 3229–3235.